Acta Geodyn. Geomater., Vol. 8, No. 3 (163), 353–369, 2011

GEOMECHANICAL PARAMETRES OF THE PODLESÍ GRANITES AND THEIR RELATIONSHIP TO SEISMIC VELOCITIES

Lucie NOVÁKOVÁ [1], Karel SOSNA [2], Milan BROŽ [1], Jan NAJSER [2] and Petr NOVÁK [3]

[1] *Institute of Rock Structure and Mechanics, Academy of Sciences of the Czech Republic, v.v.i., V Holešovičkách 41, 182 09 Prague, Czech Republic*
[2] *ARCADIS Geotechnika Ltd., Prague, Czech Republic*
[3] *Isatech Co. Ltd., Prague, Czech Republic*
**Corresponding author's e-mail:* lucie.novakova@irsm.cas.cz

(*Received* January 2011*, accepted* September 2011)

ABSTRACT
We studied the geophysical, physical, and geomechanical parameters of the Podlesí granites in the western part of the Krušné hory Mts., near the village of Potůčky. The granites represent a fractionated intrusion within the Nejdecký Massif. In total, the studied borehole is about 300 m deep. The samples were collected at depths of between 35 and 105 metres. Seismic P-wave and S-wave velocities were measured using ultrasonic scanning. The samples were water-saturated, unsaturated, and dried. The ultrasonic scanning system consisted of four piezoelectric sensors and a digital oscilloscope recorder. The wave frequency was 1 MHz. P-wave velocities range from 4400 $m.s^{-1}$ to 6500 $m.s^{-1}$ while S-wave velocities range from 2800 $m.s^{-1}$ to 3800 $m.s^{-1}$. These data were used to calculate dynamic Young's modulus, dynamic shear modulus, and Poisson's ratio. The deformational characteristics of the rock were specified from experimental loading of the sample with uniaxial strain. The shear and longitudinal deformation of each sample was measured using a resistive strain gauge fixed directly on the sample. Intermittent loading of the samples proceeded using a uniform gradient of axial stress of 1 $MPa.s^{-1}$. The samples were subjected to five separate loads. During the tests, following parameters were recorded: stress, longitudinal deformation, and shear deformation. These data were used to calculate static Young's and shear modulus, and Poisson's ratio.

KEYWORDS: granite, porosity, seismic waves, Young's modulus, shear modulus, Poisson's ratio

1. INTRODUCTION

The physical properties of crustal rocks are strongly influenced by the presence of cracks and fractures. The mechanical properties of the rocks are dependent on their fabric, texture, structure, and degree of weathering (Akesson et al., 2001). The porosity and permeability of deep-seated rocks have been shown to be more sensitive to pressure than surface samples (Morrow and Lockner, 1997). Moore and Lockner (1995) used confining pressure to create a shear fracture in a granite cylinder so as to study the microcrack pattern that related to the deformation. Lajtai (1998) demonstrated compaction and permanent damage along grain boundaries under high compression. Evans (1990) traced microfracture propagation during deformation in naturally deformed rocks. Janssen et al. (2001) used uniaxial compressive tests to form shear fractures. Akesson et al. (2001) highlighted that microfracture propagation during deformation can be either intragranular (within grains) or intergranular (through grain boundaries). In feldspars and quartz, intragranular microfractures are most common whereas micas have intergranular crack propagation. All these studies found that intragranular cracking was the dominant type of crack.

Many studies of the physical and geochemical properties of granite focus on, for example, industrial or radioactive waste disposal. However, many anthropogenic structures such as dams, bridges, or tunnels, have been constructed in granite. Chaki et al. (2008) described the study of granite microstructure and their physical and mechanical properties. It was seen that these characteristics are important for understanding damage processes and foreseeing their *in situ* evolution under various stresses. Low permeability of the rock massif is ideal when an underground gas container, fuel bin, or subsurface radioactive waste repository is planned (Sosna et al., 2009). Vaněček et al. (2010) stated the presumed safety of radioactive waste disposal in granite is based on the assumed impermeability of the granite mass. In contrast, present studies show that granites are not as impermeable as previously supposed. The aim of this work is to contribute into a general knowledge of granite properties and how these change with depth within the borehole.

Table 1 Geochemical analysis of the granite within borehole PTP-4a (Rukavičková et al., 2009).

Depth [m]	23	40	81	102
SiO_2	72.2	73.78	73.32	74.14
TiO_2	0.05	0.06	0.04	0.06
Al_2O_3	15.13	14.55	14.63	14.17
Fe_2O_3	0.31	0.51	0.16	0.47
FeO	0.66	0.68	0.64	0.54
MnO	0.032	0.028	0.023	0.02
MgO	0.06	0.14	0.03	0.09
CaO	0.71	0.39	0.52	0.39
Li_2O	0.202	0.085	0.183	0.084
Na_2O	4.29	2.99	4.08	3.29
K_2O	3.94	4.94	4.50	5.01
P_2O_5	0.687	0.245	0.507	0.285
CO_2	<0.01	<0.01	0.03	<0.01
F	1.537	0.452	1.006	0.643
S	<0.005	<0.005	<0.005	<0.005
H_2O+	1.08	1.40	0.8	1.03
H_2O-	0.18	0.35	0.13	0.19
Total [%]	**100.44**	**100.42**	**100.17**	**100.16**

2. GEOLOGICAL SETTINGS

The studied locality is situated near the settlement of Podlesí, about 2 km from Potůčky in the Krušné hory Mts., close to the border with Germany (Fig. 1: left). The Podlesí granite forms part of the late-Variscian Eibenstock-Nejdek pluton (Breiter, 2002; Müller et al., 2002). Breiter (2005) indicated the Podlesí granite is the youngest intrusion in the pluton with an age of 313 to 310 Ma. Föster (2001) stated the Podlesí granite intruded Ordovician phyllites and biotite granite at approximately 320 Ma. The vicinity of the granite comprises ordovic chlorite-sericitic phyllites with insets of quartzites and biotite granites. The contact between granite and phyllites is rather sharp (Rukavičková et al., 2009).

The internal structure of the granite massif was studied following drilling by the Czech Geological Survey (e.g. Lhotský et al., 1988; Breiter, 2001). Nine boreholes with depths of up to 350 metres have been drilled in the Podlesí granite. This paper focuses specifically on borehole PTP-4a. Albite-protholith ("granite stock") and albite-zinwaldite granite ("dyke granite") occur in the upper one hundred metres of the borehole. Between 100 and 239 metres, biotite granite is most abundant. Below 239 metres, the albite-protholith and albite-zinwaldite granite are again observed (Fig. 1: right) (Rukavičková et al, 2009).

Geochemical analysis of the PTP-4a granite has been published by Rukavičková et al. (2009). Table 1 shows the chemical composition of three different PTP-4a granites at four depth levels. Zinwaldite granite occurs at 23 m, protolith granite occurs at 40 m and 81 m, and finally biotite granite occurs at 102 m. Despite no significant differences observed between the two protolith granites, a modal analysis (Table 2) has been recalculated from the chemical composition at 30, 40, 60, 63, 72, 81, and 92 m. This reveals two different amounts of (recalculated) albite and quartz in the PTP-4a protolith granite.

3. METHODOLOGY

3.1. PREPARATION OF THE SAMPLES

Samples were taken from the granite core of borehole PTP-4a. The core diameter is 47 mm with samples taken at depths of 35 m, 45 m, 55 m, 65 m, 75 m, 85 m, 95 m, 99 m, and 105 m. The samples were cut into cylinders with lengths of either 50 mm or 100 mm. Figure 2 shows all samples taken from the upper 100 metres. This equidistant sampling strategy allows detailed analyses of the geophysical, physical,

Table 2 Modal analysis of granite within borehole PTP-4a. The mineral composition has been recalculated from the geochemical analyses.

Depth [m]	**30**	**40**	**60**	**63**	**72**	**81**	**92**	**102**
albite	22	25	33	34	34	34	33	27
protolithionit	6	5	6	6	6	6	6	5
K-felspar	25	26	25	23	24	24	24	27
topaz	1	1	5	4	5	4	4	2
quartz	44	41	29	30	30	30	31	37
akcesories	2	2	2	2	2	2	2	2
sericite	0	3	0	0	0	0	0	2
Total [%]	**100**	**103**	**100**	**99**	**101**	**100**	**100**	**102**

and geomechanical parameters of the granite within the borehole. Water saturated, unsaturated, and dried samples were studied. Unsaturated samples are granites in their 'natural' state having been stored under laboratory conditions for a few years. Saturated samples have been immersed in water for 48 hours under laboratory conditions. After measurements had been taken from the unsaturated and saturated samples, all were dried in a ventilated oven at 105 °C for 24 hours according to established standards for porosity measurements (ISRM, 1977). Samples that have been oven dried at 105 °C are considered not to be affected by cracking, and this temperature is usually used as a reference state for investigations of thermal damage (Chaki et al., 2008). The effects of heating to this temperature should be negligible as the temperature change occurs as a slow process and the thermal gradient inside the sample is low. The effect of heating of samples to 90 °C has been studied by Suzuki et al. (1998). Samples were immersed in water and no change in porosity was observed even when heated for up to 100 days. During our study, a gradual change in temperature of 0.3 °C/min was instigated during heating and cooling to prevent any cracking of the specimens due to a high temperature gradient within the specimens (Reuschlé et al., 2006; Chaki et al., 2008). During cooling, samples were kept in a closed desiccator until the room temperature was reached in order to prevent the samples coming into contact with air humidity.

3.2. ULTRASONIC SCANNING

Ultrasonic scanning is a quick and effective method used to determine the structure of a rock. P-wave and S-wave velocities were measured using an apparatus that consists of two pairs of piezosensors that used as a transmitter and receiver respectively (Fig. 3), a precise impulse generator, and an oscilloscope. The resonance frequency of the sensors was 1 MHz (Nováková et al., 2010). The contact between the sensors and sample was improved using a contact couplant. Figure 4 provides two examples of a wave travel time reading. The two vertical cursors show an original impulse and the first arrival of the received signal. Each sample was tested in three perpendicular directions to assess anisotropy. The first direction was always the vertical axis of a core (and the borehole) whilst the other two were set up visually, one parallel to observed mineral anisotropy (if there was any) and the other perpendicular to it.

Dynamic Young's modulus E_d (Eq. 1), shear modulus G_d (Eq. 2), and Poisson's ratio (Eq. 3; Zisman, 1933) were calculated.

$$E_d = \frac{\rho v_S^2 \left(3v_P^2 - 4v_S^2\right)}{v_P^2 - v_S^2} \tag{1}$$

$$G_d = \rho v_S^2 \tag{2}$$

$$v = \frac{v_P^2 - 2v_S^2}{2\left(v_P^2 - v_S^2\right)} \tag{3}$$

where E_d is dynamic Young's modulus, ρ is density of the studied sample, v_s is S-wave velocity, v_p is P-wave velocity, G_d is shear modulus, v is Poisson's ratio.

3.3. DEFORMABILITY IN UNIAXIAL COMPRESSION

This method determines the elastic parameters of rock. Cylindrical rock samples (47 × 100 mm) were loaded using uniaxial stress. During the experiment both sample deformations, transverse and longitudinal, were recorded by resistivity tensometers (20/120LY41 Hottinger Baldwin Messtechnik) attached to its surface (Fig. 5). Loading was performed in five cycles with a constant gradient of 1 MPa.s^{-1}. The loading maximums were set to 20, 30, 40, 50, and 60 % of the compressive strength. The unloading minimum was set to 5 % of the compressive strength. Young's modulus and Poisson's ratio were calculated following the methodology of

Zavoral et al. (1987). Poisson's ratio was determined from hysteresis of first and second loading loop (Eq. 4).

$$\nu = \frac{\frac{\varepsilon_{d1} + \varepsilon_{d3}}{2} - \varepsilon_{d2}}{\frac{\varepsilon_{a1} + \varepsilon_{a3}}{2} - \varepsilon_{a2}} \quad (4)$$

where ε_{ai} and ε_{di} are appropriate average values of longitudinal and transverse deformation respectively, and ν is Poisson's ratio. Finally, stress was applied up to the strength limit.

3.4. DRY DENSITY AND POROSITY

The dry density was determined following Zavoral et al. (1987)

$$\rho_d = \frac{m_{d1}}{V} \quad (5)$$

where ρ_d is dry density of the sample, m_{d1} is weight after first drying, and V is volume.

The volume (V) of the sample was obtained by weighing in air (m_v) and in water (m_v')

$$V = \frac{m_v - m_v'}{\rho_t} \quad (6)$$

where ρ_t is water density.

The porosity (n) was obtained by weighing the saturated (m_{sat}) and dry (m_d) samples, respectively

$$n = \frac{m_{sat} - m_d}{V \rho_t} \quad (7)$$

where ρ_t is water density and V volume of the sample. Weighting was always performed in identical conditions following the methodology ISRM (1977).

4. RESULTS

4.1. SEISMIC VELOCITIES

P-wave velocities (see Fig. 6) vary according to the depth of sample and the level of saturation. The highest were recorded in the saturated samples (5750 m.s^{-1} to 6536 m.s^{-1}, blue lines) while the lowest were recorded in the dry samples (4387 m.s^{-1} to 5387 m.s^{-1}, red lines). However, each curve follows the same trend. Fig. 6 clearly demonstrates the high level of isotropy across the samples. In particular, the dry samples show practically the same velocities in all measured directions. Some anisotropy was identified in the saturated samples where P-wave velocities in coaxial direction of the sample (originally vertical in the borehole) are slightly higher (up to 5 % in the highest velocity samples) than in the other directions (originally horizontal in the borehole). The unsaturated samples provide similar results, except that the coaxial velocities are up to 5 % lower in the highest velocity samples.

S-wave velocities (see Fig. 7) also vary according to the sample depth and level of saturation. In the saturated samples, S-wave velocities were found to be higher (3262 m.s^{-1} to 3815 m.s^{-1}) than in dry samples (2844 m.s^{-1} to 3425 m.s^{-1}). Both curves again show similar trends. S-wave velocities in the unsaturated samples varied considerably (2982 m.s^{-1} to 3752 m.s^{-1}).

The level of saturation affects both P-wave and S-wave velocities. The difference in P-wave velocities between dry and saturated samples was as much as 20 %. The difference in S-wave velocities was slightly lower at less than 15 %.

4.2. YOUNG'S MODULUS

The trend of dynamic Young's modulus (see Fig. 8) follows that of the seismic wave velocities. It varies from 67.0 GPa to 96.3 GPa in the saturated samples, from 47.5 GPa to 72.3 GPa in the dried samples, and from 52.2 GPa to 85.4 GPa in the unsaturated samples. The samples show directional anisotropy but this again rather insignificant. As with the velocities, the modulus was found to be higher in the saturated samples than in dry samples. The difference in moduli between the saturated and dry samples is about 30 %.

The unsaturated samples were used for static Young's modulus assessment. The modulus was found to range from 31.4 GPa to 57.1 GPa (Fig. 9: green line). The figure, however, presents an apparent link between the static modulus and the dynamic modulus of the dry samples. Despite the shift in values, a notable correlation is clear.

4.3. SHEAR MODULUS

Figure 10 shows that the shear modulus ranges from 27.2 GPa to 38.2 GPa in the saturated samples, from 22.6 GPa to 36.8 GPa in the unsaturated samples, and from 22.0 GPa to 30.7 GPa in the dried samples. The shear modulus of the saturated samples is clearly higher than the shear modulus of the dried samples. Directional anisotropy of the modulus is present although it is not significant. There is remarkable similarity between the curves derived for the shear modulus and those derived for Young's modulus (see Fig. 9).

The unsaturated samples were used to determine the static shear modulus, despite the fact that the best correlation is derived from the dynamic shear modulus of the dried samples. Calculated from static Young's modulus and Poisson's ratio, the static shear modulus of the unsaturated samples ranges from 13.0 GPa to 23.4 GPa (Fig. 11: green line).

4.4. POISSON'S RATIO

Poisson's ratio was defined using the ultrasonic scanning method and loading tests. For the unsaturated samples, the average value of Poisson's ratio was 0.16 (0.05-0.23), for the saturated samples it was 0.25 (0.18-0.27), and for the dried samples it was

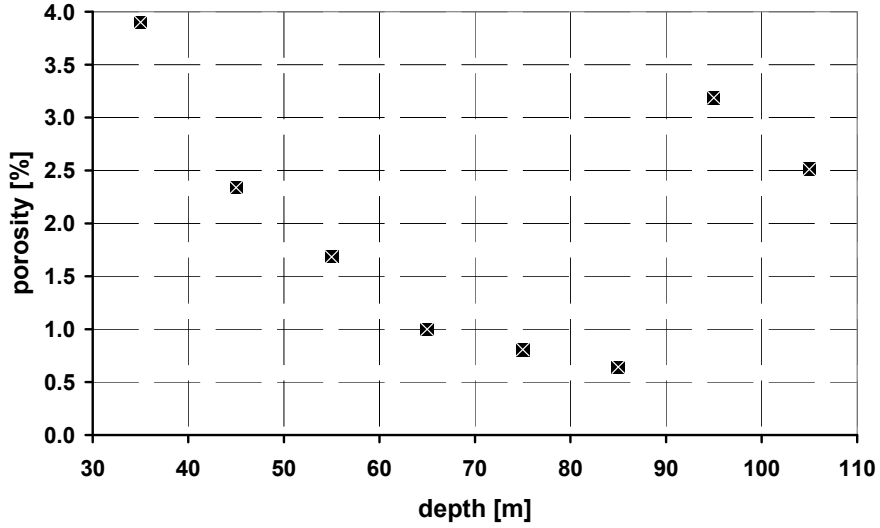

Fig. 15 The relationship between sample porosity and depth within the borehole.

0.17 (0.11-0.22) (Fig. 12). The average value of Poisson's ratio for the unsaturated samples was 0.21, calculated from uniaxial loading. Although the trends were generally similar, the curves vary significantly in detail (see Fig. 13). Nonetheless, the strongest correlation was provided by the static curve and the dynamic curve derived from ultrasonic scanning for the dried samples.

4.5. DRY DENSITY AND POROSITY

The P-wave and S-wave velocities correlate well with the dry sample densities (Fig. 14). An increase in velocity of about 600 meters per second was identified for every increase in density of 100 kg.m^{-3}. The porosity of the samples is described in Figure 15. Sample porosity decreases with depth within the borehole. However, the two deepest samples (95 m and 105 m) have higher porosity. This is particularly important for understanding the decrease in velocities of these samples (see Figs. 6 and 7) in addition to explaining their Young's and shear moduli (see Figs. 8 to 11). Fig. 16 shows a remarkable relationship between porosity and seismic wave velocity in the samples. It is obvious that porosity influences both ultrasonic velocities and moduli. However, the porosity of the PTP-4a granite depends on the (recalculated) amount of albite (cf. Table 2 and Fig. 15). The positive correlation between porosity and albite suggests that the presence of albite seems to be a major factor in determining porosity within the granites of borehole PTP-4a.

5. DISCUSSION AND CONCLUSIONS

The main advantages of ultrasonic scanning are its low cost compared to other methods such as uniaxial loading or drilling and the rapidity with which large amounts of data can be processed. Seismic measurements are able to find relatively small anomalies in the physical parameters within one featureless borehole. A further advantage is that it is possible to assess deformation parameters perpendicular to the borehole. It is not always possible to measure such parameters in these two directions using uniaxial loading, especially in small-profiled cores.

All the obtained data demonstrate a correlation between the properties of the granite and depth within the borehole. Except for lowermost ~ 10 metres in which the protolith granite changes to biotite granite, the same rock type occurs in the studied part of borehole PTP-4a. A transition zone between these granites is quite easy to demonstrate using seismic velocities. P-wave and S-wave velocities are remarkably lower in samples below 90 metres. Nevertheless, the progression of seismic velocities with the depth in the borehole is not explicit. Chaki et al. (2008) stated that the ultrasonic wave propagation is in reciprocal proportion with the overall damage of the material. To assess all possible aspects, anisotropy was studied in the granite rocks. P-wave velocities do not show any anisotropy in the studied samples, their velocities vary from 4387 m.s^{-1} to 6536 m.s^{-1} while S-wave velocities vary from 2844 m.s^{-1} to 3815 m.s^{-1}. The highest velocities were consistently measured in the saturated samples while the lowest velocities were consistently measured in the dried samples. This is unsurprising given that P-wave velocity in water is almost four times higher than it is in air. This is much the same for dry density and, therefore, P-wave velocities also relate to dry density.

Zhao and Li (2000) found that changes in Young's modulus were rather small compared with the change in tensile strength with the loading rate. During compaction, caused by axial microcracking,

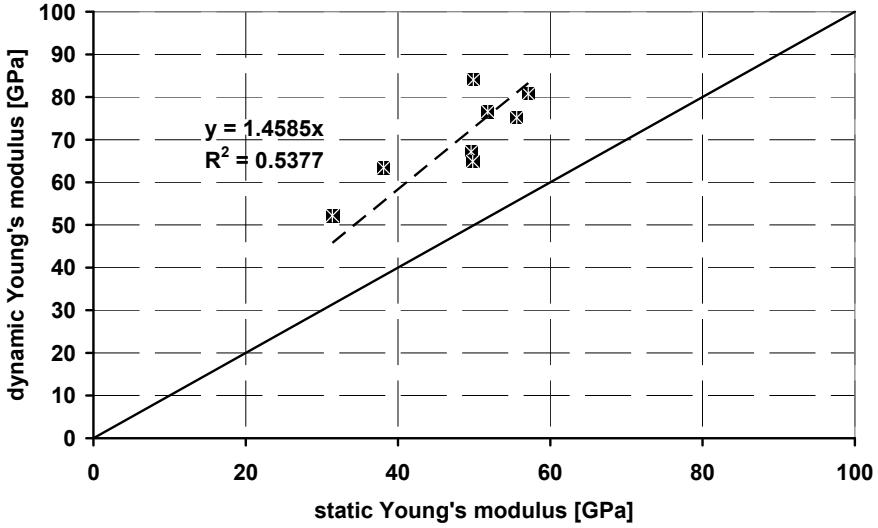

Fig. 17 The correlation between static and dynamic Young's modulus (unsaturated samples, only vertical direction).

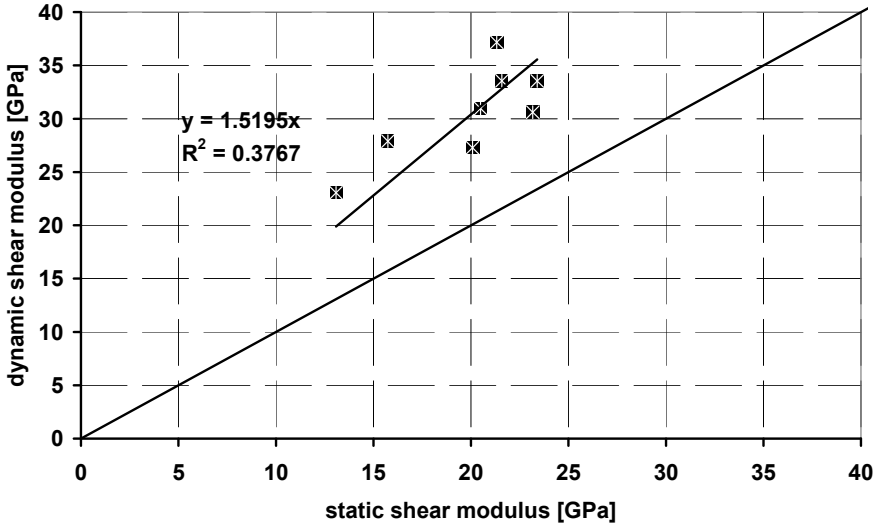

Fig. 18 The correlation between static and dynamic shear modulus (unsaturated samples, only vertical direction).

the axial stiffness (elastic modulus) of the rock increases (Lajtai, 1998). Uniaxial compressive strength rises with depth and varies from 85 MPa to 155 MPa. The highest values represent the depths of about 100 metres. Gere and Timoshenko (1997) described Young's modulus for granite in range from 40 GPa to 100 GPa. We separated Young's modulus according to method that was calculated. Dynamic Young's modulus varies from 47.5 GPa to 96.3 GPa while static Young´s modulus varies from 31.4 GPa to 57.1 GPa. Dynamic Young's modulus is approximately 1.5 higher than static Young's modulus (Fig. 17). Dynamic and static shear moduli show a similar relationship. Dynamic shear modulus is approximately 1.5 higher than static shear modulus (Fig. 18). Dynamic shear modulus varies from 22.0 GPa to 38.2 GPa whilst static shear modulus varies from 13.0 GPa to 23.4 GPa. Gere and Timoshenko (1997) recorded Poisson's ratio for granites of between 0.2 and 0.3. Poisson's ratio also changes with the depth. We have recorded Poisson's ratio between 0.16 and 0.25. The porosity of the studied granites decreases with depth until 85 metres. However, at about 100 metres, the porosity increases. The highest porosity was found to be about 3.9 % while the lowest was about 0.6 %. The PTP-4a granite matrix porosity correlates very well with the quantity of albite, which probably contains a significant amount of pores.

All the data point to the same conclusions. With depth there are increases in seismic velocities,

Young's modulus, static modulus, dry density, and compressive strength. With depth the porosity decreases. Poisson's ratio is not influenced significantly by depth. These conclusions specifically relate to the protolith granite within borehole PTP-4a. At a depth of about 90 metres, there is a transition zone between the protolith granite and the biotite granite. This transition zone markedly influences data derived from depths below ~ 85 m. Rukavičková et al. (2009) put the zone at a depth of 100 m. The results presented here suggest that this transition zone is in fact wider than previously supposed. It would, therefore, be useful to study the influence of saturation on the static modulus in order to compare it with the dynamic modulus.

ACKNOWLEDGEMENTS

This work was funded by the Ministry of Industry and Trade of the Czech Republic (FR-TI1/367) and the Institute of Rock Structure and Mechanics AS CR, v.v.i. (A VOZ30460519). We are grateful to our friends and colleagues, the Czech Geological Survey, Progeo s.r.o., and UJV Řež a.s. for participating on the project, "Research of an influence of a granite matrix porosity over a radioactive waste geological disposal safety including methodology and measuring devices development" (http://www.granite-porosity.cz). The authors would thank to Karel Breiter for calculating a modal analyses. The authors are grateful to unknown reviewers for their constructive comments and suggestions. Matt Rowberry provided a critical revision of the English.

REFERENCES

Akesson, U., Lindqvist, J.E., Göransson, M. and Stigh, J.: 2001, Relationship between texture and mechanical properties of granites, central Sweden, by use of image-analysing techniques. Bulletin of Engineering Geology and the Environment, 60, 277–284.

Bieniawski, Z.T.: 1967, Mechanism of brittle fracture of rock. Parts I. and II. International Journal of Rock Mechanics and Mining Sciences, 3, 395–423.

Breiter, K.: 2001, Phosphorus- and fluorine-rich granite system at Podlesí. In: Breiter K. (ed.) Phosphorus- and Fluorine-rich Granites. Abstracts, excursion guide, and program. International Workshop Podlesí, Czech Geological Survey, Praha, 54–78.

Breiter, K.: 2002, From explosive breccia to unidirectional solidification textures: magmatic evolution of a phosphorusand fluorine-rich granite system (Podlesí, Krušné Hory Mts., Czech Republic). Bulletin of the Czech Geological Survey, 77, 67–92.

Breiter, K., Müller, A., Leichmann, J., and Gabašová, A.: 2005, Textural and chemical evolution of a fractionated granitic system: the Podlesí stock, Czech Republic. Lithos, 80, 323–345.

Chaki, S., Takarli, M. and Agbodan, W.P.: 2008, Influence of thermal damage on physical properties of a granite rock: porosity, permeability and ultrasonic wave evolutions. Construction and Building Materials, 22, 1456–1461.

Evans, J.P.: 1990, Textures, deformation mechanisms, and the role of fluids in the cataclastic deformation of granitic rocks. In Knipe, R.J. and Rutter, E.H. (eds.) Deformation Mechanisms, Rheology and Tectonics. Special Publication of the Geological Society of London, 200, 29–39.

Föster, H.J.: 2001, The radioactive accessory-mineral assemblage of the Podlesí granite-pegmatite system, western Krušné hory: implications to intrusion age and magmatic/hydrothermal fluid-rock interaction. In: Breiter, K., (ed.) Phosphorus- and Fluorine-rich Granites. Abstracts, excursion guide, and program. International Workshop Podlesí, Czech Geological Survey, Praha, 14–15.

Gere, J.M. and Timoshenko, P.S.: 1997, Mechanics of Materials. 4th ed. Boston: PWS Publishing Company.

ISRM.: 1977, Suggested methods for determining water content, porosity, density, absorption and related properties and swelling and slake-durability index properties. I.S.R.M. Suggested Methods.

Janssen, C., Wagner, F.C., Zang, A. and Dresen, G.: 2001, Fracture process zone in granite: a microstructural analysis. International Journal of Earth Sciences (Geol. Rundsch.), 90, 46–59.

Lajtai, E.Z.: 1998, Microscopic fracture processes in a granite. Rock Mechanics and Rock Engineering, 31, 237–250.

Lhotský, P., Breiter, K., Bláha, V. and Hrochová, H.: 1988, Economic-geological investigations of Sn-mineralisation near Podlesí in the western Krušné hory. Internal Report, Czech Geological Survey, Praha (in Czech).

Moore, D.E. and Lockner, D.A.: 1995, The role of microcracking in shear-fracture propagation in granite. Journal of Structural Geology, 17, 95–114.

Morrow, C.A. and Lockner, D.A.: 1997, Permeability and porosity of the Illinois UPH 3 drillhole granite and a comparison with other deep drillhole rock. Journal of Geophysical Research, 102, B2, 3067-3075.

Müller, A., Kronz, A., and Breiter, K.: 2002, Trace elements and growth patterns in quartz: a fingerprint of the evolution of the subvolcanic Podlesí Granite System (Krušné Hory, Czech Republic). Bulletin of the Czech Geological Survey, 77, 135–145.

Nováková L., Brož, M. and Novák, P.: 2010, Comparative study of geophysical parameters and geochemical analysis in undisturbed granites. In Williams et al. (eds.) Geologically Active. Taylor & Francis Group, London, 2281–2288.

Reuschlé, T., Gbaguidi Haore, S. and Darot, M.: 2006, The effect of heating on the microstructural evolution of La Peyratte granite deduced from acoustic velocity measurements. Earth and Planetary Science Letters, 243, 692–700.

Rukavičková, L., Breiter, K., Holeček, J., Pačes, T., Procházka, J., Hanák, J., Dobeš, P., Havlová, V., Večerník, P. and Hercík, M.: 2009, Dílčí zpráva č.: 1.4 Etapová zpráva o řešení projektu v roce 2009. Výzkum vlivu mezizrnné propustnosti granitů na bezpečnost hlubinného ukládání do geologických formací a vývoj metodiky a měřící aparatury, FR-TI1/367, 130.

Schild, M., Siegesmund, S., Vollbrecht, A. and Mazurek, M.: 2001, Characterization of granite matrix porosity and pore-space geometry by in situ and laboratory

methods. Geophysical Journal International, 146, 111–125.

Sosna, K., Brož, M., Vaněček, M. and Polák, M.: 2009, Exploration of a granite rock fracture system using a TV camera. Acta Geodynamica et Geomaterialia, 6, 453–463.

Suzuki, K., Oda, M., Yamazaki, M., Kuwahara, T.: 1998, Permeability changes in granite with crack growth during immersion in hot water. International Journal of Rock Mechanics and Mining Science, 35, 907-921.

Vaněček, M., Trpkošová, D., Polák, M., Sosna, K., Michálková, J., Novák, P., Milický, M., Gvožík, L., Záruba, J. and Navrátil, T.: 2010, Matrix permeability of granite rocks and validation of modelling solution. In Williams et al. (eds.) Geologically Active. Taylor & Francis Group, London, 3765–3772.

Zavoral, J.: 1987, Techniques of laboratory tests in mechanics of soils and rocks. Mechanics of the Soil: Techniques (in Czech). Ústřední ústav geologický, Praha, 186.

Zisman, W.A.: 1933, Comparison of the statically and seismologically determined elastic constants of rocks. Geology, 19, 680–686.

Zhao, J. and Ki, H.B.: 2000, Experimental determination of dynamic tensile properties of a granite (technical note). International Journal of Rock Mechanics and Mining Science, 37, 861–866.

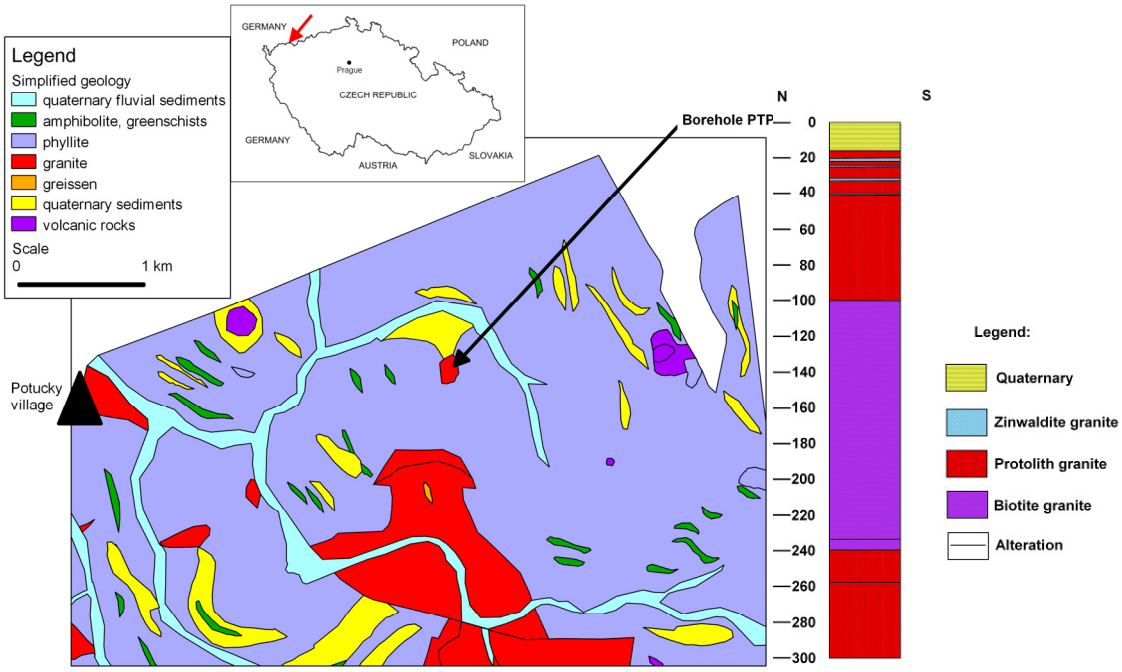

Fig. 1 A schematic geological map of the studied locality (left, modified after Czech Geological Survey, 2010) and a schematic geological profile of borehole PTP-4a (right, modified after Rukavičková et al., 2009).

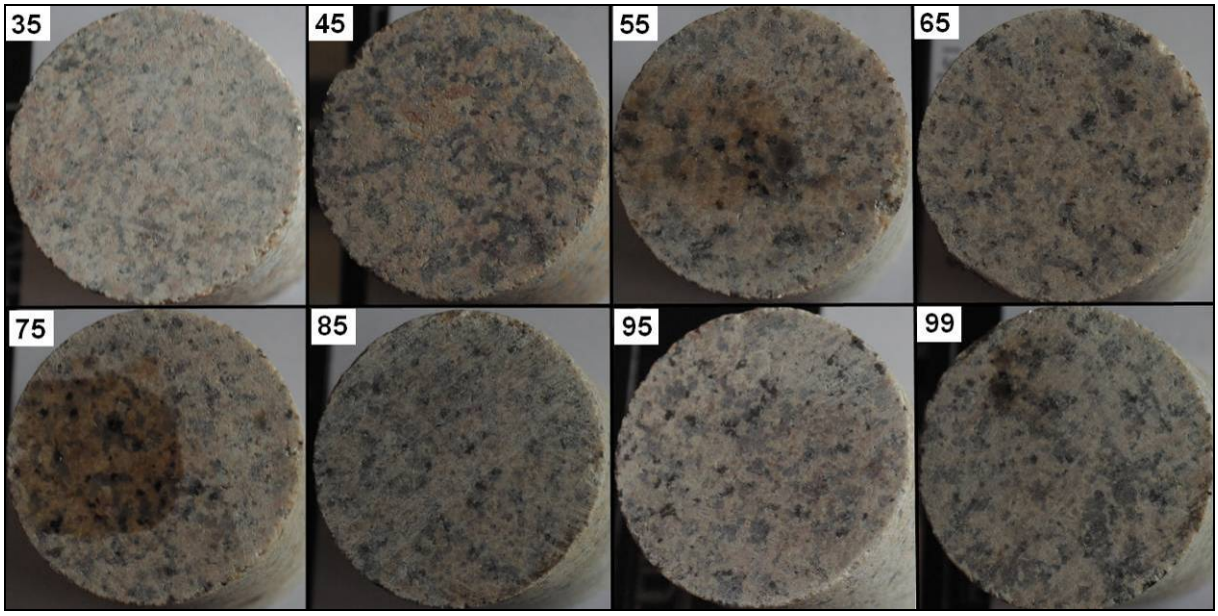

Fig. 2 Photographs of the granite core samples from borehole PTP-4a. The numbers reflect the depth of the sample within the borehole (m).

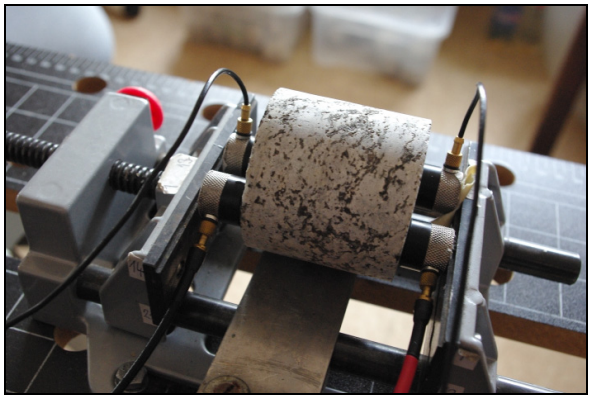

Fig. 3 Piezoelectric sensors on the granite core sample (Olympus V103 and V153). The two sensors at the front generate P-waves, the two sensors at the back generate S-waves.

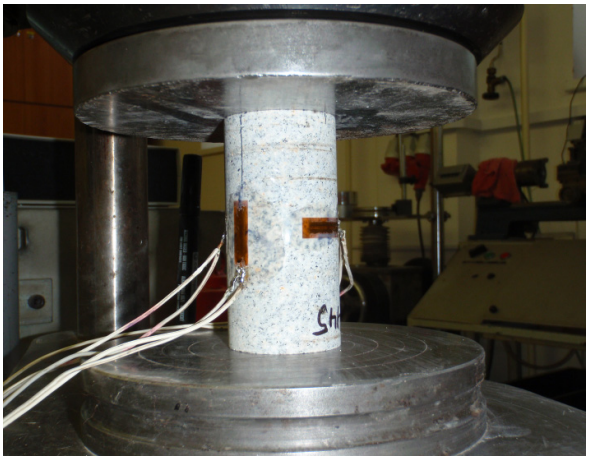

Fig. 5 Resistant tensometres placed directly on the sample during uniaxial loading.

Fig. 4 Arrival time of P-wave (left) and arrival time of S-wave (right).

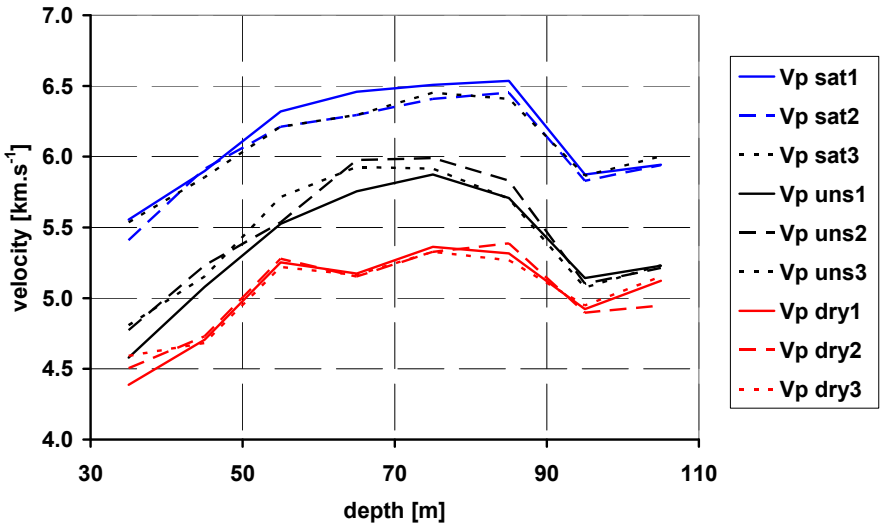

Fig. 6 P-wave velocities of the studied granite samples: black - unsaturated samples; blue - saturated samples; red - dried samples.

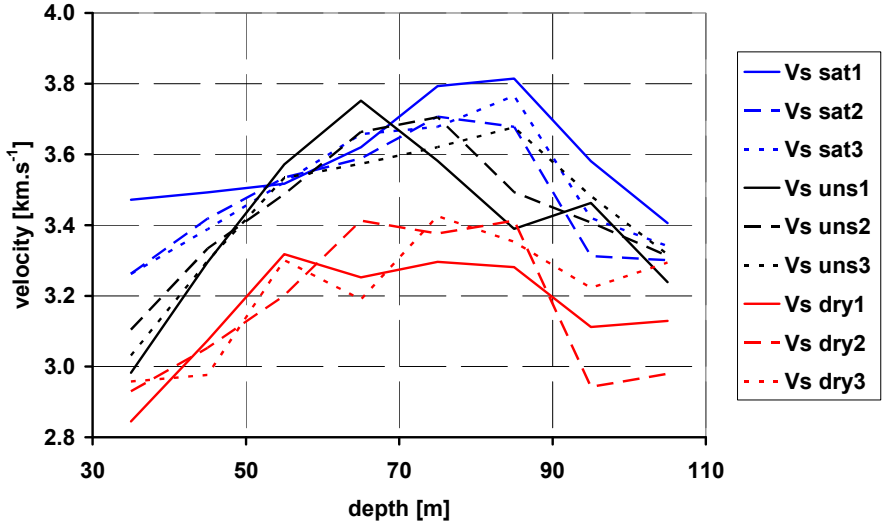

Fig. 7 S-wave velocities of the studied granite samples: black - unsaturated samples; blue - water saturated samples; red - dried samples.

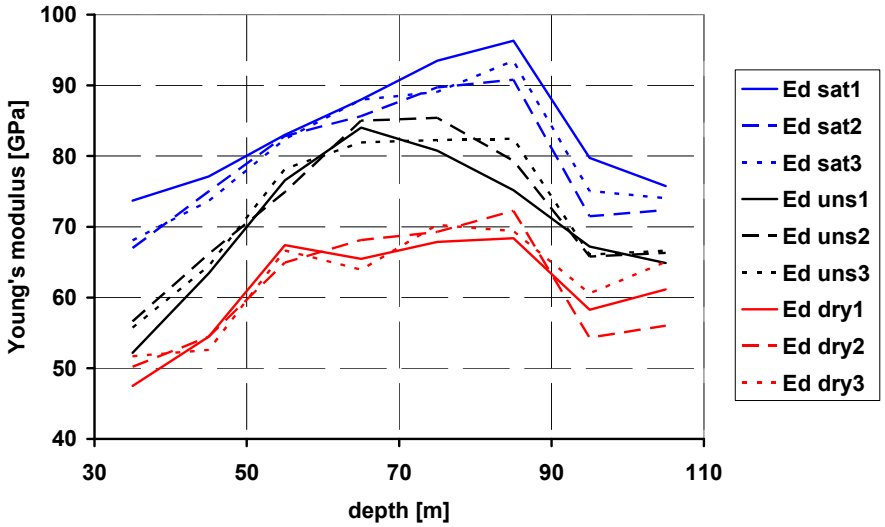

Fig. 8 The relationship between dynamic Young's modulus with sample depth within the borehole: black - unsaturated samples; blue - saturated samples; red - dried samples.

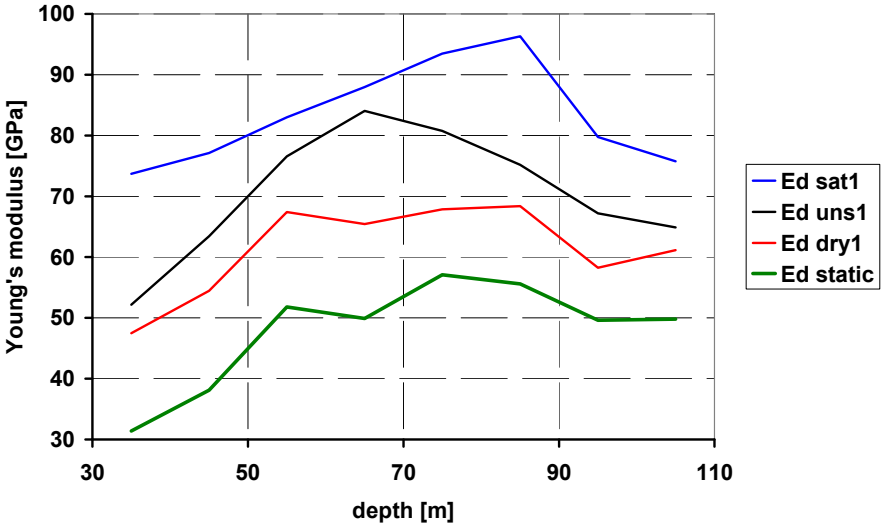

Fig. 9 The relationship between static Young's modulus and dynamic Young's modulus with sample depth within the borehole. Static Young's modulus: green - unsaturated samples. Dynamic Young's modulus: black - unsaturated samples; blue - saturated samples; red - dried samples.

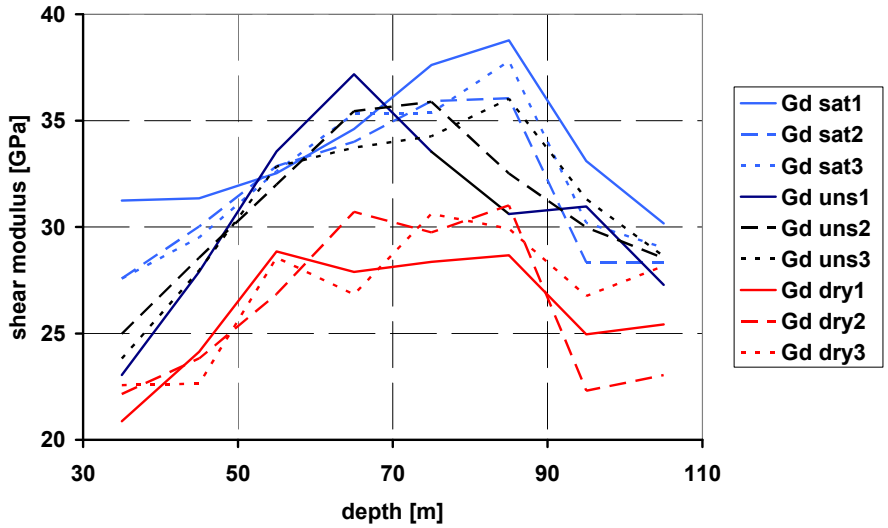

Fig. 10 The relationship between shear modulus with sample depth within the borehole: black - unsaturated samples; blue - saturated samples: red - dried samples.

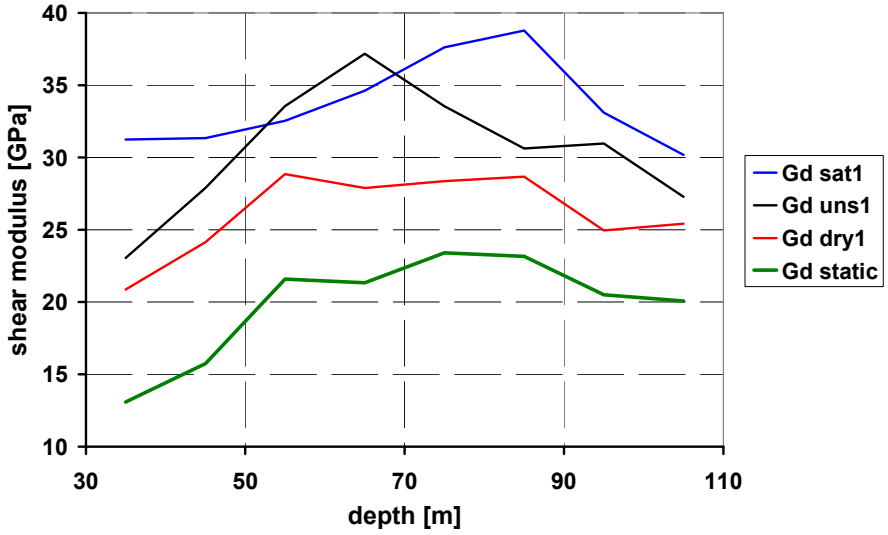

Fig. 11 The relationship between static shear modulus and dynamic shear modulus with sample depth within the borehole. Static shear modulus: green - unsaturated samples. Dynamic shear modulus: black - unsaturated samples; blue - saturated samples; red - dried samples.

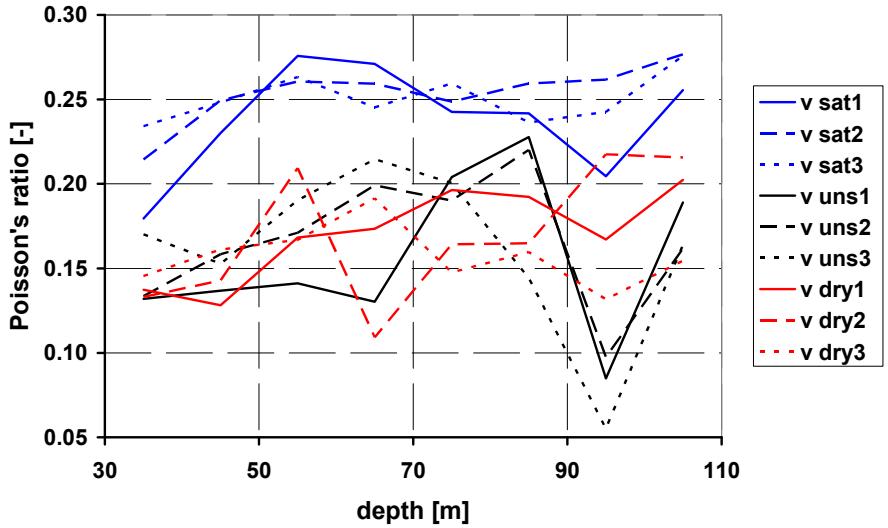

Fig. 12 The relationship between Poisson's ratio and sample depth within the borehole: black - unsaturated samples; blue - water saturated samples; red - dried samples.

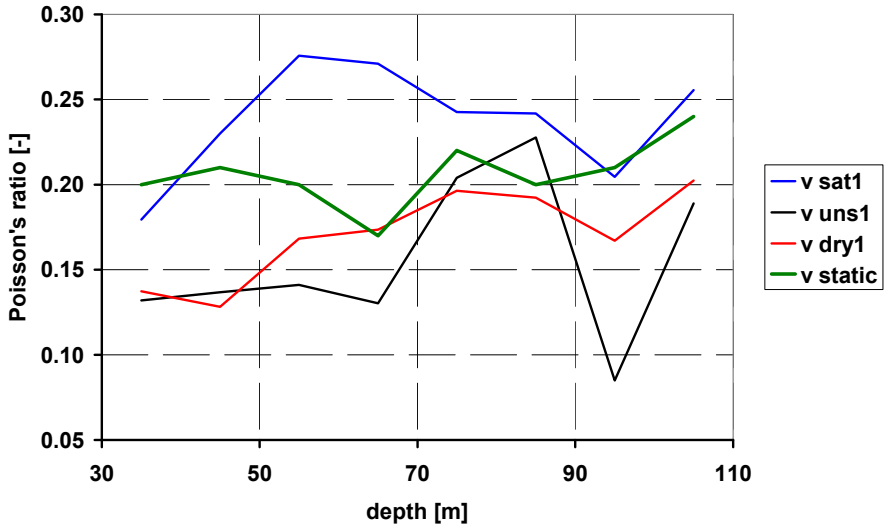

Fig. 13 The relationship between Poisson's ratio and sample depth within the borehole. Poisson's ratio calculated from uniaxial loading: green - unsaturated samples. Poisson's ratio calculated from ultrasonic scanning: black - unsaturated samples; blue - saturated samples; red - dried samples.

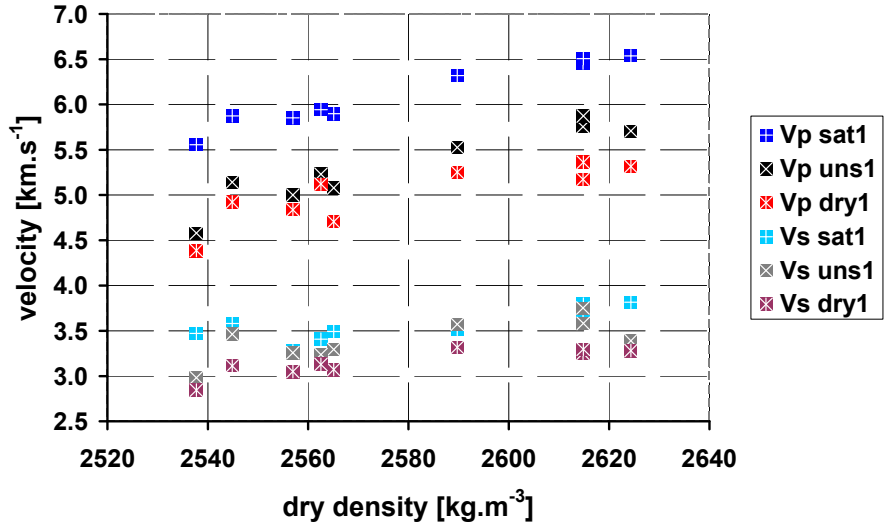

Fig. 14 The relationship between P-wave and S-wave velocities with dry density. Dark blue: P-wave velocities of saturated samples; black: P-wave velocities of unsaturated samples; red: P-wave velocities of dried samples; light blue: S-wave velocities of saturated samples; grey: S-wave velocities of unsaturated samples; dark red: S-wave velocities of dried samples.

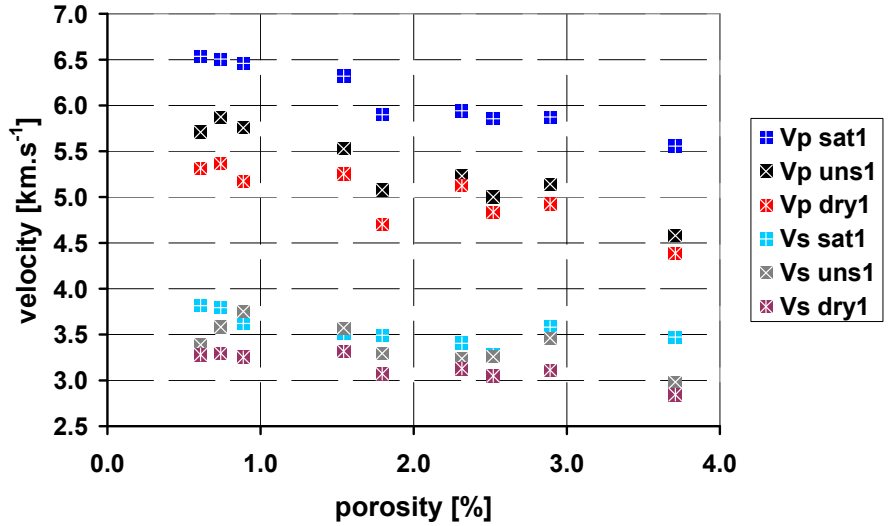

Fig. 16 The relationship between seismic velocities and porosity for the studied samples. Dark blue: P-wave velocities of water saturated samples; black: P-wave velocities of unsaturated samples; red: P-wave velocities of dried samples; light blue: S-wave velocities of saturated samples; grey: S-wave velocities of unsaturated samples; dark red: S-wave velocities of dried samples.